Redox Biology 65 (2023) 102828

Contents lists available at ScienceDirect

Redox Biology

journal homepage: www.elsevier.com/locate/redox

Epigenetic modulation of Drp1-mediated mitochondrial fission by inhibition of S-adenosylhomocysteine hydrolase promotes vascular senescence and atherosclerosis

Yiran You [a], Xu Chen [b], Yu Chen [a], Juan Pang [a], Qian Chen [c,d], Qiannan Liu [a], Hongliang Xue [a], Yupeng Zeng [a], Jinghe Xiao [a], Jiaxin Mi [a], Yi Tang [e], Wenhua Ling [a,d,f,*]

[a] Department of Nutrition, School of Public Health, Sun Yat-Sen University, Guangzhou, People's Republic of China
[b] Department of Molecular, Cellular and Developmental Biology, University of Colorado, Boulder, USA
[c] Department of Cardiology, Sun Yat-sen Memorial Hospital, Sun Yat-sen University, Guangzhou, People's Republic of China
[d] School of Public Health and Management, Ningxia Medical University, Yinchuan, People's Republic of China
[e] Department of Nutrition, The First People's Hospital of Zhaoqing, Zhaoqing, China
[f] Guangdong Provincial Key Laboratory of Food, Nutrition and Health, Guangzhou, People's Republic of China

ARTICLE INFO

Keywords:
vascular senescence
Atherosclerosis
S-adenosylhomocysteine hydrolase
DNA methylation
mitochondrial dynamics

ABSTRACT

Aims: Vascular senescence, which is closely related to epigenetic regulation, is an early pathological condition in cardiovascular diseases including atherosclerosis. Inhibition of S-adenosylhomocysteine hydrolase (SAHH) and the consequent increase of S-adenosylhomocysteine (SAH), a potent inhibitor of DNA methyltransferase, has been associated with an elevated risk of cardiovascular diseases. This study aimed to investigate whether the inhibition of SAHH accelerates vascular senescence and the development of atherosclerosis.

Methods and results: The case-control study related to vascular aging showed that increased levels of plasma SAH were positively associated with the risk of vascular aging, with an odds ratio (OR) of 3.90 (95% CI, 1.17–13.02). Elevated pulse wave velocity, impaired endothelium-dependent relaxation response, and increased senescence-associated β-galactosidase staining were observed in the artery of *SAHH*$^{+/-}$ mice at 32 weeks of age. Additionally, elevated expression of p16, p21, and p53, fission morphology of mitochondria, and over-upregulated expression of Drp1 were observed in vascular endothelial cells with SAHH inhibition *in vitro* and *in vivo*. Further down-regulation of Drp1 using siRNA or its specific inhibitor, mdivi-1, restored the abnormal mitochondrial morphology and rescued the phenotypes of vascular senescence. Furthermore, inhibition of SAHH in *APOE*$^{-/-}$ mice promoted vascular senescence and atherosclerosis progression, which was attenuated by mdivi-1 treatment. Mechanistically, hypomethylation over the promoter region of *DRP1* and downregulation of DNMT1 were demonstrated with SAHH inhibition in HUVECs.

Conclusions: SAHH inhibition epigenetically upregulates Drp1 expression through repressing DNA methylation in endothelial cells, leading to vascular senescence and atherosclerosis. These results identify SAHH or SAH as a potential therapeutic target for vascular senescence and cardiovascular diseases.

1. Introduction

Atherosclerosis is a chronic disease of vascular intima and is a leading cause of morbidity and mortality worldwide [1]. Vascular aging caused by cellular senescence is a major risk factor for atherosclerosis [2]. Especially, endothelial senescence, has been observed in the early stages of atherosclerosis and shown to be involved in its pathogenesis [3]. Senescent vascular cells release higher levels of proinflammatory cytokines and less NO, thus initiating atherosclerosis, while senolytic drugs [4] and phytochemicals [5,6] are able to improve cellular dysfunction and ameliorate the development of atherosclerosis. In recent years, in addition to classical stimuli such as free radicals and toxins, it has been suggested that epigenetics is another regulator of vascular senescence, but the mechanism remains largely unknown [7].

Mitochondria are organelles with dynamic morphology maintained by an equilibrium between fission and fusion. Imbalanced

* Corresponding author. School of Public Health, Sun Yat-Sen University (Northern Campus), No.74, 2nd Zhongshan Road, Guangzhou, 510080, PR China.
E-mail address: lingwh@mail.sysu.edu.cn (W. Ling).

https://doi.org/10.1016/j.redox.2023.102828
Received 14 July 2023; Accepted 24 July 2023
Available online 25 July 2023

mitochondrial dynamics cause an accumulation of reactive oxygen species (ROS), ATP depletion, and mitochondrial DNA (mtDNA) damage, resulting in cellular senescence [8,9]. In mammalian cells, dynamin-related protein 1 (Drp1) and fission 1 (Fis1) are key proteins regulating mitochondrial fission, while optic atrophy 1 (OPA1) and mitofusin1&2 (MFN1&2) can modulate mitochondrial fusion [10]. Aberrant changes in these molecules are related not only to cellular senescence [11] and shortened lifespan [12] but also to vascular diseases [13], indicating the critical role of mitochondrial dynamics in age-dependent diseases such as cardiovascular diseases (CVDs).

S-adenosylhomocysteine (SAH) is produced from S-adenosylmethionine (SAM) in methylation reactions. S-adenosylhomocysteine hydrolase (SAHH) is the only enzyme which catalyzes the reversible hydrolysis of SAH to adenosine and homocysteine, maintaining methylation-related epigenetics and homeostasis in the methionine cycle [14]. Inhibition of SAHH results in higher levels of intracellular and plasma SAH and is tied to atherosclerosis in both epidemiological research and laboratory studies [15–18]. Considering that vascular senescence is associated with epigenetics but the mechanism is unclear, we postulated that SAHH inhibition can induce vascular senescence and thereby accelerate atherosclerosis. Previous studies of our group have shown that SAHH inhibition was associated with senescence in human umbilical vein endothelial cells [19], however, the mechanism was not verified in further *in vivo* models and remained elusive. Herein, we investigated the impact of SAHH inhibition on vascular senescence in the context of atherosclerosis. Our study shows that inhibition of SAHH can induce vascular senescence through epigenetic upregulation of Drp1-mediated mitochondrial fission and therefore, accelerate the progression of atherosclerosis.

2. Methods and materials

2.1. Case-control study

The protocols of human study were approved by the Institutional Review Board of the Sun Yat-sen University (No. SYSU-SPH-2021-126). All procedures performed in this study were in accordance with the principles outlined in the Declaration of Helsinki. Written informed were obtained from all participants. The study population was selected from the Guangzhou Nutrition and Health Study (GNHS), which targeted middle-aged and elderly individuals (40–80 years old) residing in southern China. Case subjects were defined by a brachial ankle pulse wave velocity (baPWV) $\geq$ 1400 cm/s, measured using a BP-203RPEIII detector (OMRON, Tokyo, Japan). Control subjects were matched to case subjects by age (within 3 y) and sex. Participants with hepatic or renal failure, cancer, chemotherapy or the use of anticancer agents were excluded from the study. Carotid intima-media thickness (cIMT) and flow-mediated dilation (FMD) were also measured in the study participants. cIMT was measured using a high-resolution 7.0–12.0-MHz linear-array transducer system (Apoli:Toshiba, Tokyo, Japan) according to the manufacturer's guidelines. FMD in the brachial artery was measured with a UNEXEF18G ultrasound system (OMRON, Tokyo, Japan), also following the manufacturer's guidelines. Blood samples were collected and stored at −80 °C for further analysis.

2.2. Animal experiments

All animal studies were approved by the institutional Animal Care and Use Committee of the School of Public Health of Sun Yat-sen University (No. SYSU-SPH-2020-013) and conducted in compliance with the National Institutes of Health (NIH) guidelines for the Care and Use of Laboratory Animals. Heterozygous SAHH knockout mice ($SAHH^{+/-}$) were bred with apolipoprotein E-deficient mice ($APOE^{-/-}$) to produce $APOE^{-/-}SAHH^{+/-}$ mice. Male mice were maintained in SPF conditions under a controlled 12-h light/dark cycle and temperature at 22 ± 2 °C, with *ad libitum* access to water and food. Mice were euthanized with sodium pentobarbital (200 mg/kg, i.p.) and tissues were collected for further studies.

2.2.1. Experiment 1

To investigate the effect of SAHH inhibition on vascular senescence, male $SAHH^{+/-}$ mice at age of 8 weeks and wild type littermates (n = 6) were fed a chow diet for 24 weeks.

2.2.2. Experiment 2

To confirm that vascular senescence induced by SAHH inhibition was mediated by mitochondria-derived reactive oxygen species (mtROS), male $SAHH^{+/-}$ mice at age of 8 weeks and wild type littermates were divided into four groups (n = 6): wild type + saline (i.p.) group, wild type + mitoTEMPO group (i.p. 0.5 mg/kg every other day), $SAHH^{+/-}$ + saline (i.p.) group, and $SAHH^{+/-}$ + mitoTEMPO group (i.p. 0.5 mg/kg every other day). These mice were fed a chow diet for 24 weeks.

2.2.3. Experiment 3

To explore the role of Drp1 in vascular senescence induced by SAHH inhibition, male $SAHH^{+/-}$mice at age of 8 weeks and wild type littermates were divided into four groups (n = 6): wild type + saline (i.p.) group, wild type + mdivi-1 (i.p. 10 mg/kg twice a week) group, $SAHH^{+/-}$ + saline (i.p.) group, and $SAHH^{+/-}$ + mdivi-1 (i.p. 10 mg/kg twice a week) group. These mice were fed a chow diet for 24 weeks.

2.2.4. Experiment 4

To investigate the association among SAHH inhibition, vascular senescence, and atherosclerosis progression, male $APOE^{-/-}$ mice at age of 8 weeks were divided into three groups (n = 6) and fed a western diet fed (D12079B, Research Diets, New Brunswick, NJ) for 0, 6, and 12 weeks, respectively.

2.2.5. Experiment 5

To verify whether SAHH inhibition accelerates atherosclerosis in a Drp1-dependent manner, male $APOE^{-/-}SAHH^{+/-}$ mice at age of 8 weeks and their $APOE^{-/-}$ littermates were divided into four groups (n = 6): $APOE^{-/-}$group, $APOE^{-/-}$ + mdivi-1 group (i.p. 10 mg/ml twice a week); $APOE^{-/-}SAHH^{+/-}$group, and $APOE^{-/-}SAHH^{+/-}$ + mdivi-1 group (i.p. 10 mg/ml twice a week). These mice were fed a western diet (D12079B, Research Diets, New Brunswick, NJ) for 8 weeks.

2.3. Determination of SAH and SAM

The concentrations of intracellular and mouse plasma SAH and S-adenosylmethionine (SAM) were determined as previously described [20].

2.4. Transmission electron microscopy (TEM)

HUVECs were dispersed with 0.25% trypsin and centrifuged at 1000 rpm for 5 min. After removing the supernatant, the cell pellet was fixed with 2.5% glutaraldehyde at room temperature for 30 min and 4 °C for preservation. The cells were then dehydrated and embedded with EMBed 812 (SPI) for polymerization at 65 °C for 48 h. Sections (70 nm) were cut, counterstained with methanolic uranyl acetate and lead citrate, and photographed using a transmission electron microscope (HT7800, Hitachi, Tokyo, Japan). Fresh aorta of mice was cut into 2-mm-long rings and fixed with 2.5% glutaraldehyde at room temperature for 30 min and preserved at 4 °C. Subsequent procedures were the same as those used for HUVECs.

2.5. MitoTracker green and MitoSOX staining

MitoTracker Green (Invitrogen, Carlsbad, CA, USA) at a working concentration of 100 nM in endothelial cell medium was used to stain cells at 37 °C for 20 min. After replacing the staining solution with fresh

medium, the cells were photographed at 490 nm (Ex)/516 nm (Em) using a confocal laser microscope (Leica, Wetzlar, Germany). MitoSOX (Invitrogen, Carlsbad, CA, USA) at 1 μM in HBSS buffer was used to stain cells at 37 °C, protected from light for 10 min. The cells were gently washed with warm HBSS buffer for three times and photographed at 510 nm (Ex)/580 nm (Em) using a confocal laser microscope (Leica, Wetzlar, Germany).

2.6. In vitro methylation assay

The Drp1 promoter plasmid (100 μg) were mixed with 500 μl of NEB buffer (NEB, Ipswich, MA, USA), 500 μl of 1600 μM SAM, 400 units of Sss1 methyltransferase and nuclease-free water (up to 5 ml). The mixture was then incubated at 37 °C for 1 h and 65 °C for 20 min to terminate the reaction. The same amount of plasmid DNA was incubated without the enzyme as a control.

2.7. Immunohistochemistry

Frozen sections of mouse aorta were fixed with 4% paraformaldehyde (Biosharp, Beijing, China) for 15 min, permeabilized with 0.5% Triton X-100 (Biosharp, Beijing, China) in PBS for 10 min and then incubated with 3% H_2O_2 to quench endogenous peroxidase. The sections were rinsed with PBS for 2 × 3 min and blocked with goat serum at room temperature for 30 min. The sections were then incubated with anti-CD31 antibody (1:100, Cell Signaling Technology, Danvers, MA) at 4 °C overnight, followed by the addition of a peroxidase-conjugated goat anti-rabbit secondary antibody (1:200, Servicebio, Wuhan, China) at room temperature for 30 min. Specific proteins were detected with DAB, and counterstained with hematoxylin for 5 s. The sections were then visualized using a light microscope (Leica, Wetzlar, Germany).

2.8. Dihydroethidium (DHE) staining

Fresh aortic cross-sections (30 μm) were equilibrated in Krebs buffer for 30 min at 37 °C and then incubated with dihydroethidium (3 μM) for 30 min at 37 °C, protected from light. Images were obtained using a confocal laser microscope (Leica, Wetzlar, Germany) and analyzed using LAS AF software (Leica, Wetzlar, Germany).

2.9. MitoTEMPO treatment

A 50 mM stock solution of mitoTEMPO (MCE, Monmouth Junction, NJ, USA) was prepared by dissolving it in water. Subsequently, HUVECs were treated with a working solution of 50 μM mitoTEMPO in complete medium at 37 °C for 24 h.

2.10. Amplicon bisulfite sequencing

Genomic DNA of HUVECs was extracted with a genomic DNA extraction kit (Tsingke, Beijing, China). Bisulfite conversion of the genomic DNA (2 μg) was performed according to the manufacturer's protocol supplied with the EZ DNA Methylation Gold Kit (Zymo Research, Orange, CA, USA). Specific primers for the promoter regions of the Drp1 gene were designed (E-gene Co. Ltd, Shenzhen, China) and used to perform bisulfite PCR amplification and library construction. Integrity and quantification were tested using Agilent 2100 and Qubit 2.0. Then, sequencing was performed in an Illuminia system. Alignment was conducted in reference to the Drp1 gene sequence from NCBI.

2.11. Western blot analysis

Proteins from HUVECs were extracted with RIPA lysis buffer (Beyotime, Shanghai, China) containing 1% PMSF (Beyotime, Shanghai, China) and quantified using a BCA protein assay kit (Thermo Fisher Scientific, Waltham, MA, USA). Equal amounts of protein (30 μg) were separated by 10% sodium dodecyl sulfate polyacrylamide gel electrophoresis (SDS-PAGE), transferred to 0.22-μm PVDF membranes (Millipore, Billerica, MA, USA), and incubated overnight at 4 °C with specific antibodies: *anti*-p16, *anti*-p21, *anti*-FIS1, *anti*-SAHH (Abcam, Cambridge, UK), *anti*-p53, *anti*-Drp1, *anti*-OPA1, *anti*-MFN1, *anti*-MFN2, *anti*-DNMT1, *anti*-DNMT3A, *anti*-DNMT3B, and *anti*-GAPDH (Cell Signaling Technology, Danvers, MA) followed by incubation with horseradish peroxidase-conjugated secondary antibodies (Cell Signaling Technology, Danvers, MA). The dilution ratio was 1:1000 for the primary antibodies and 1:10,000 for the secondary antibodies. Protein bands were visualized with Super Signal Chemiluminescence Substrate (Thermo Scientific, Waltham, MA, USA) and GAPDH was used as a control. Images were captured using the FluorChem E system (Protein Simple, Minneapolis, MN, USA) and band densities were quantified using image J software (NIH, Bethesda, MD, USA). The densities of the bands were normalized to that of GAPDH.

2.12. Senescence-associated β-galactosidase (SA β-gal) staining

The senescence of endothelial cells (ECs) and aorta was measured using a senescence-associated β-galactosidase (SA β-gal) staining kit (Beyotime, Shanghai, China). The protocol was conducted according to the manufacturer's guide. In brief, HUVECs were seeded in a 6-well plate. Upon confluency, cells were fixed and incubated with SA β-gal working solution overnight in a non-humidified CO_2-free incubator at 37 °C. Random images per well were captured using light microscopy. SA β-gal positive cells were manually counted, and the total cell number per field was quantified using image J software (NIH, Bethesda, MD, USA). Aorta was harvested from sacrificed mice and perfused with ice-cold PBS. The subsequent procedures were the same as those used for HUVECs.

2.13. Statistics

The results are presented as means ± SEMs. The statistical significance between groups was determined using two-tailed unpaired Student's *t*-test, Mann-Whitney *U* test, or one-way ANOVA followed by Bonferroni post hoc tests as appropriate. A probability value less than 0.05 was considered statistically significant. Logistic regression and Spearman correlation analysis was performed for the case-control study. SPSS 25.0 software (IBM Corporation, Armonk, NY, USA) were used for all statistical analyses.

3. Results

3.1. Plasma SAH levels are associated with vascular aging in the population

To investigate the association between SAH metabolism and vascular aging in human, a case-control study enrolling 102 age- and sex-matched participants was conducted. Cases were defined as brachial ankle pulse wave velocity (ba-PWV) ≥ 1400 cm/s. Descriptive statistics are listed in Supplementary Table 1. As shown in Fig. 1A–C, plasma SAH levels were significantly higher and SAM/SAH ratio were lower in the case group compared with the control group, but plasma SAM levels did not differ between groups. The logistic regression indicated that plasma SAH level was a risk factor for vascular aging, with an adjusted odds ratio (OR) (95% confidence interval, CI) of 3.90 (1.17–13.02) for Tertile 3 vs. Tertile 1 (Table 1). In addition, the spearman correlation analysis showed that plasma SAH levels was positively correlated with ba-PWV ($r = 0.314$, $P < 0.01$) (Fig. 1D), carotid intima-media thickness (cIMT) ($r = 0.290$, $P < 0.01$) (Fig. 1E) and negatively correlated with flow-mediated dilation (FMD) ($r = -0.196$, $P < 0.05$) (Fig. 1F), further suggesting a link between SAH metabolism and age-associated alterations in vasculature.

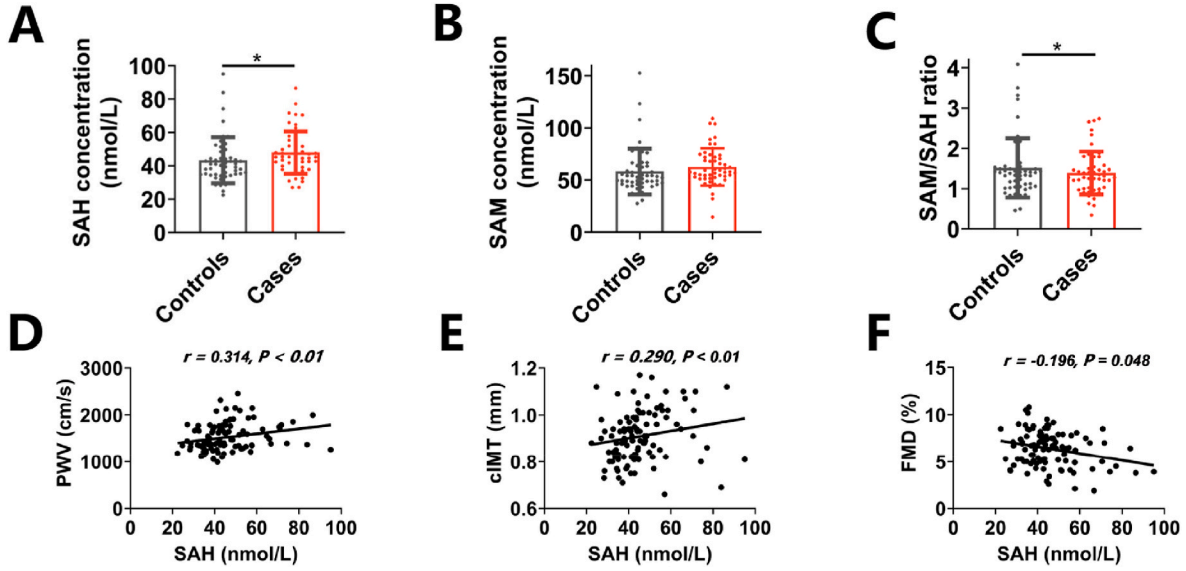

Fig. 1. Plasma SAH levels are associated with vascular aging in population
A case–control study (n = 51/group) related to vascular aging was conducted. Cases were defined as ba-PWV ≥1400 cm/s. **(A)–(C)** Differences in the levels of plasma SAH, SAM, and SAM/SAH between controls and cases. Plasma levels of SAH and SAM were measured by stable-isotope dilution liquid chromatography–electrospray tandem mass spectrometry. **(D)–(F)** The correlation between plasma SAH levels and baPWV, cIMT, and FMD in the cases and the controls. ba-PWV, brachial ankle pulse wave velocity; cIMT, carotid intima-media thickness; FMD, flow-mediated dilation. For all bar graphs, data are means ± SEM, $*p < 0.05$ (determined by the Mann-Whitney *U* test). Correlation was conducted using Spearman correlation analysis.

Table 1
Odds ratios of risk for vascular aging by plasma SAH levels.

Variables	Cases (n = 51)	Controls (n = 51)	OR (95% CI)	Adjusted OR[a] (95% CI)
SAH levels (nM)				
T1 (<39.21)	12	22		
T2 (39.21–47.46)	18	16	2.06 (0.78–5.46)	1.87 (0.59–5.93)
T3 (>47.46)	21	13	2.96 (1.10–7.94)	3.90 (1.17–13.02)

CI, Confidence interval; OR, odds ratio; T1, Tertile 1.
[a] Adjusted for age, sex, BMI, and smoking status.

3.2. SAHH inhibition induces vascular senescence

To explore whether SAHH inhibition affected vascular senescence, *SAHH*$^{+/-}$ mice were generated by CRISPR/Cas9 system and their validation was confirmed (Supplementary Figs. 2A–E). At 32 weeks of age, *SAHH*$^{+/-}$ mice exhibited higher plasma SAH levels, lower SAM/SAH ratio (Supplementary Figs. 3A–B), and displayed signs of vascular senescence, as evidenced by an increased PWV value (Fig. 2B) and impaired endothelium-dependent relaxation response (Fig. 2C). But the endothelium-independent relaxation did not alter between groups (Fig. 2C). Elevated senescence-associated β-galactosidase (SA β-gal) staining in the aorta (Fig. 2D) and increased expression of p16, p21, and p53 (Fig. 2E), markers of cellular senescence, were also observed in *SAHH*$^{+/-}$ group compared with the wild type group. Additionally, we observed that cellular senescence predominately occurred in the endothelial layer through combined β-gal staining and immunohistochemical staining of CD31, a marker of vascular endothelial cells, in sections of artery (Fig. 2D). In addition, basic phenotypes of key metabolic tissues including the liver, skeletal muscle, and epididymal adipose tissue in abovementioned mouse groups were examined and the data demonstrated no significant alterations between groups (Supplementary Figs. 2F–H). Subsequently, the human umbilical vein endothelial cells (HUVECs) from passage 3–5 were then treated with the SAHH inhibitor adenosine dialdehyde (ADA) (30 μM) or transfected with *SAHH* siRNA for 48 h, which led to reduced expression of SAHH (Supplementary Figs. 3C–D) and SAM/SAH ratio (Supplementary Fig. 3F), and increased intracellular SAH levels (Supplementary Fig. 3E). Inhibition of SAHH increased SA β-gal staining (Fig. 2F) and expression of p16, p21, and p53 in HUVECs with SAHH inhibition compared with the control group (Supplementary Figs. 3G–H). Taken together, these findings suggest that SAHH inhibition induces vascular senescence.

3.3. SAHH inhibition promotes mitochondrial fission and elevates mtROS levels

Given that SAHH inhibition is associated with DNA hypomethylation, whole-genome bisulfite sequencing (WGBS) was performed on HUVECs treated with SAHH inhibition for further mechanistic investigations (Supplementary Fig. 4A). The sequencing results revealed that the global methylation level decreased in the SAHH inhibition group compared to the control group (Supplementary Fig. 4B). Additionally, GO enrichment analysis of sequencing datasets suggested that genes regulating mitochondrial dynamics might mediate the senescence-prone effect of SAHH inhibition (Supplementary Fig. 4C). Furthermore, examination of transmission electron microscope (TEM) and staining of MitoTracker Green on HUVECs demonstrated that SAHH inhibition turned mitochondria into shorter morphologies, indicating excessive mitochondrial fission (Fig. 3A–C). *In vivo*, TEM examination on the endothelial layer of *SAHH*$^{+/-}$ mice also revealed a fission-prone morphology of mitochondria (Fig. 3E–F). As mitochondria-derived reactive oxygen species (mtROS) resulting from disturbance of mitochondrial dynamics can cause cellular senescence through DNA damage and other pathway, mtROS levels were measured in HUVECs using MitoSOX staining. The results indicated higher levels of mtROS in

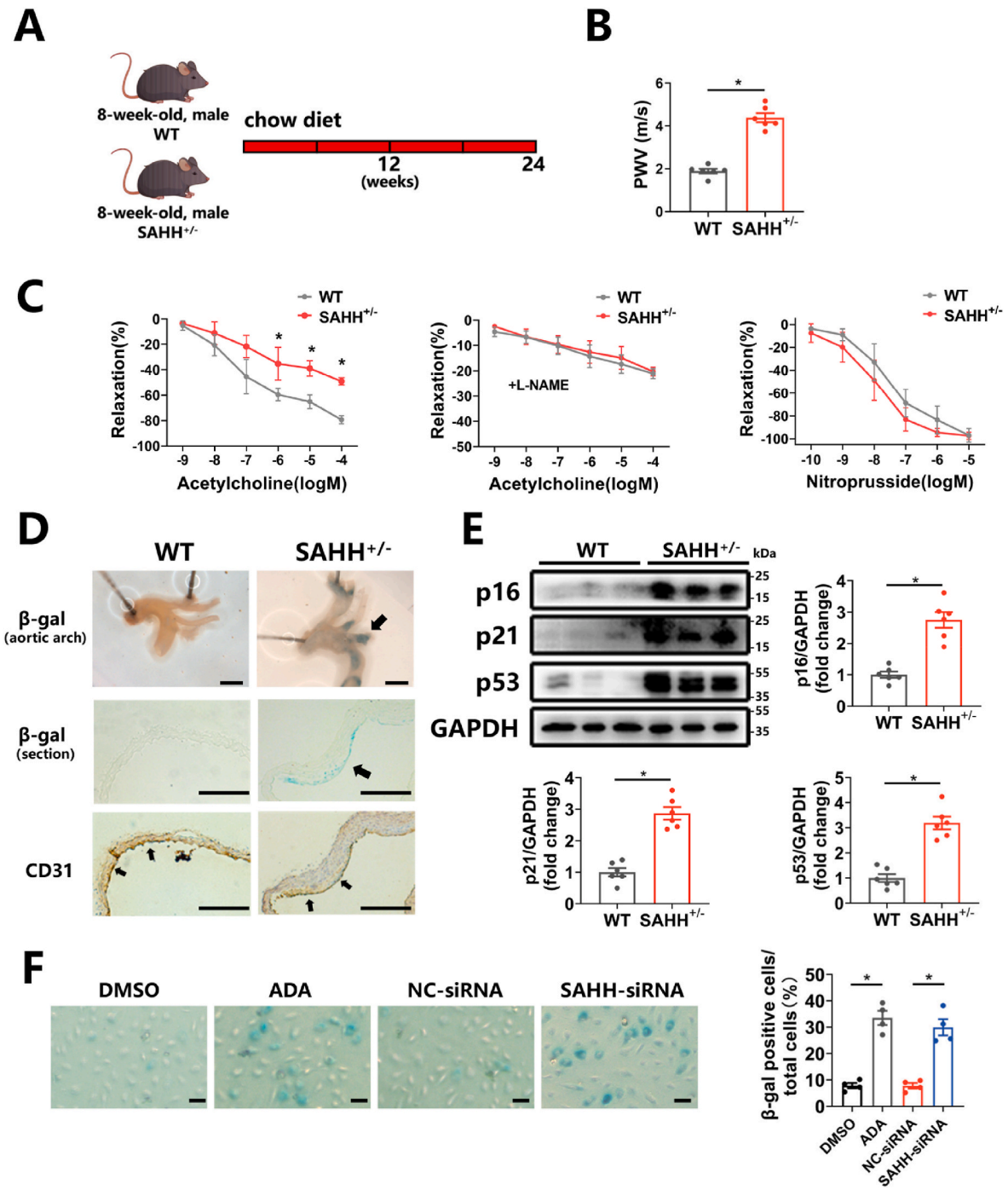

Fig. 2. SAHH inhibition induces vascular senescence.
(A) 8-week-old male *SAHH*$^{+/-}$ mice and wild type littermates were fed a chow diet for 24 weeks (n = 6). **(B)** Aortic pulse wave velocity in abovementioned mouse groups (n = 6). **(C)** Endothelium-dependent vascular relaxation in response to acetylcholine in the presence or absence of eNOS inhibitor L-NAME, and endothelium-independent vascular relaxation in response to nitroprusside in abovementioned mouse groups (n = 6). **(D)** SA β-gal staining and CD31 immunohistochemical staining in the aortic arch of abovementioned mouse groups (n = 6). Scale bar = 2 mm, 250 μm, and 250 μm (from the top to bottom). **(E)** Western blot analysis of p16, p21, and p53 protein expression in the aorta of abovementioned mouse groups (n = 6). **(F)** HUVECs were treated with ADA (30 μM) or transfected with *SAHH* siRNA for 48 h. SA β-gal staining of abovementioned HUVECs groups (n = 4). Scale bar = 200 μm. SA β-gal, senescence-associated β-galactosidase; PWV, pulse wave velocity. For all bar graphs, data are means ± SEM, *$p < 0.05$ (determined by the *t*-test).

the SAHH-inhibition group than in the control group (Fig. 3A, D). Similarly, *SAHH*$^{+/-}$ mice also showed elevated levels of ROS in the artery (Fig. 3E, G). Notably, the effect of SAHH inhibition on β-gal staining was abrogated upon mitoTEMPO administration, a specific quencher of mtROS, both *in vitro* and *in vivo* (Fig. 3H–J). Given that elevated mtROS has been reported to elicit both cellular senescence and apoptosis, TUNEL assay was performed in HUVECs with SAHH inhibition but no significant change was observed between groups (Supplementary Fig. 5A). Additionally, it is worth noting that mitochondrial fission can serve as a mechanism to segregate damaged mitochondria for further degradation through mitophagy. In light of this, we further investigated the involvement of mitophagy in HUVECs treated with SAHH inhibition

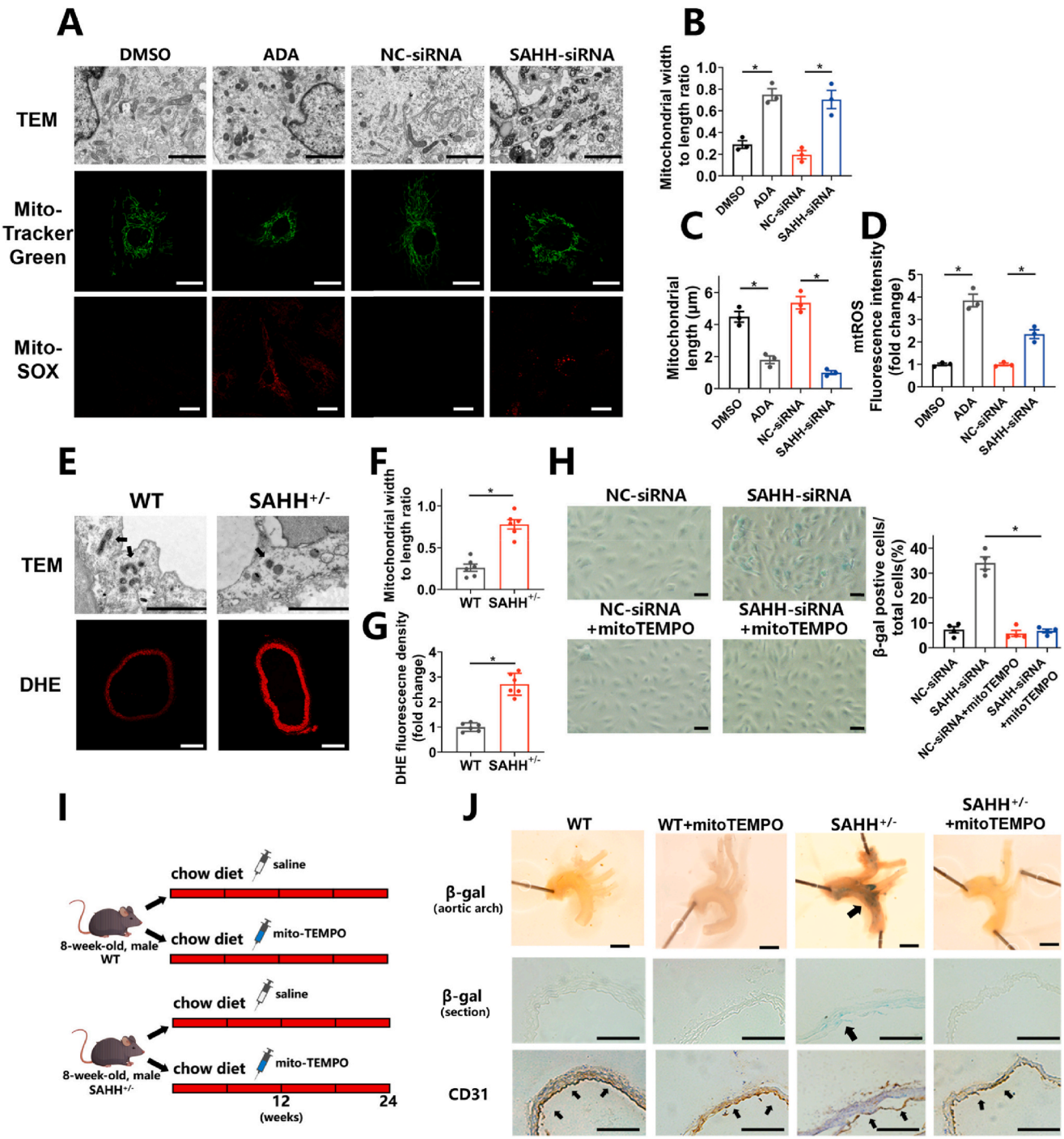

Fig. 3. SAHH inhibition promotes mitochondrial fission and elevated mtROS.
(A) Morphology of mitochondria detected by transmission electron microscopy, morphological staining of mitochondria using MitoTracker Green dye, and mtROS staininig using MitoSOX dye in HUVECs treated with ADA (30 μM) or transfected with *SAHH* siRNA for 48 h (n = 3). Scale bar = 2 μm, 25 μm, and 25 μm (from the top to bottom). **(B)** Quantification of the ratio of mitochondrial width to length according to TEM examination in **(A)**. **(C)** Quantification of the mitochondrial length according to Mitotracker Green staining in **(A)**. **(D)** Quantification of mtROS levels according to MitoSOX staining in **(A)**. **(E)** Morphology of mitochondria in the aortic endothelium detected by transmission electron microscopy and DHE staining of the aorta in wild type and $SAHH^{+/-}$ mouse groups (n = 6). Scale bar = 2 μm and 250 μm (from the top to bottom). **(F)** Quantification of the ratio of mitochondrial width to length according to TEM examination in **(E)**. **(G)** Quantification of DHE fluorescence density according to DHE staining in **(E)**. **(H)** SA β-gal staining of HUVECs transfected with *SAHH*-siRNA for 48 h in the presence or absence of mitoTEMPO (50 μM) (n = 4). Scale bar = 200 μm. **(I)** Male $SAHH^{+/-}$ mice and their wild type littermates were divided into 4 groups (n = 6): wild type group, wild type + mitoTEMPO (i.p. 0.5 mg/kg every other day), $SAHH^{+/-}$ group, and $SAHH^{+/-}$ + mitoTEMPO (i.p. 0.5 mg/kg every other day) group and fed a chow diet from 8 to 32 weeks of age. **(J)** SA β-gal staining and CD31 immunohistochemical staining of the aortic arch of the abovementioned mouse groups (n = 6). Scale bar = 2 mm, 250 μm, and 250 μm (from the top to bottom). TEM, transmission electron microscopy; SA β-gal, senescence-associated β-galactosidase; mtROS, mitochondria-derived reactive oxygen species. For all bar graphs, data are means ± SEM, $*p < 0.05$ (determined by the *t*-test or 1-way ANOVA). (For interpretation of the references to colour in this figure legend, the reader is referred to the Web version of this article.)

using Mitophagy staining and observed increased mitophagy in the SAHH inhibition group compared with the control (Supplementary Fig. 5B).

3.4. Endothelial senescence induced by SAHH inhibition is mediated through the Drp1-mtROS pathway

To further explore the mechanism by which SAHH inhibition induce mitochondrial fission, the expression of key molecules regulating mitochondrial dynamics was tested in HUVECs with SAHH inhibition. The results showed that the expression of Drp1 was upregulated by 71.9% and 73.3% at the mRNA level and by 2.06 times and 2.44 times at the protein level in the ADA-treated and siRNA-treated groups, respectively, compared with control groups (Supplementary Fig. 5C and Fig. 4A). Whereas the expression of Fis1, OPA1, MFN1 and MFN2 remained unaltered (Supplementary Fig. 5C and Fig. 4A). Likewise, the protein level of Drp1 was increased by 2.15 times in the aorta of $SAHH^{+/-}$ mice compared with that of wild-type mice (Fig. 4B). To further investigate the role of Drp1 in SAHH inhibition-induced mitochondrial fission and cellular senescence, *DRP1* siRNA or mdivi-1 (a Drp1 inhibitor) were used to inhibit Drp1 *in vitro* and *in vivo*, respectively (Fig. 4C and Supplementary Fig. 5D). The results showed that inhibition of Drp1 recovered the shape of mitochondria in SAHH-inhibited HUVECs and endothelium of $SAHH^{+/-}$ mice to baseline levels (Fig. 4D–F, 4I-J). Furthermore, knocking down Drp1 with siRNA abrogated the mtROS elevation in HUVECs (Fig. 4D, G) and mdivi-1 treatment alleviated the ROS levels in the artery of $SAHH^{+/-}$ mice (Fig. 4I, K). However, quenching mtROS with mitoTEMPO did not affect Drp1 expression or mitochondrial morphology in HUVECs with SAHH inhibition (Supplementary Figs. 5E–F), suggesting that mtROS was increased in a Drp1-dependent fashion, but not the other way round. The knockdown of Drp1 also attenuated the SA β-gal staining in HUVECs with SAHH inhibition (Fig. 5A) and reduced protein expression of p16, p21, and p53 in HUVECs transfected with siRNA by 54.5%, 55.5%, and 43.8%, respectively (Fig. 5B). *In vivo*, inhibition of Drp1 ameliorated endothelial senescence and vascular senescence in $SAHH^{+/-}$ mice by decreasing PWV value (Fig. 5C), improving endothelium-dependent relaxation response (Fig. 5D), and reducing SA β-gal staining (Fig. 5E). The protein expression of p16, p21, and p53 in the aorta of $SAHH^{+/-}$ mice treated with mdivi-1 was also reduced by 67.0%, 61.9%, and 67.4% respectively compared with the control (Fig. 5F–G). These findings suggests that inhibition of SAHH induce endothelial senescence and vascular senescence via the Drp1-mtROS pathway.

3.5. SAHH inhibition accelerates atherosclerosis via a Drp1-dependent pathway

To verify whether the aforementioned mechanisms apply to the development of atherosclerosis, we conducted further investigations in $APOE^{-/-}$ mice. Utilizing a model of atherosclerosis involving $APOE^{-/-}$ mice fed a western diet (Fig. 6A), our findings revealed increases in SA β-gal staining of the artery, protein expression levels of p16, p21, and p53 in the aorta, and plaque formation in male $APOE^{-/-}$ mice over a 12-week period of western diet feeding (Fig. 6 B, E). Concurrently, plasma levels of SAH were elevated by 2.91 times, while plasma SAM/SAH ratio was reduced by 63.4% in the 12-week mouse group compared to the 0-week group (Fig. 6C–D). Furthermore, protein expression of SAHH in the aorta decreased by 33.3% in the 6-week group and by 62.6% in the 12-week group, relative to the 0-week group (Fig. 6E). Protein expression of Drp1 in the aorta was increased by 51.6% in the 6-week mouse group and by 2.27 times in the 12-week group, compared to the 0-week group (Fig. 6E). These findings suggest that SAHH declined and phenotypes related to vascular senescence increased in $ApoE^{-/-}$ mouse model during a western-diet feeding and the progression of atherosclerosis. Subsequently, $APOE^{-/-}SAHH^{+/-}$ mice were generated by breeding $SAHH^{+/-}$ knockout mice with $APOE^{-/-}$ mice and identified with agarose gel electrophoresis (Supplementary Fig. 6A). At the age of 8 weeks, male $APOE^{-/-}SAHH^{+/-}$ mice and their $APOE^{-/-}$ littermates were divided into 4 groups: $APOE^{-/-}$group, $APOE^{-/-}$ + mdivi-1(i.p.) group, $APOE^{-/-}SAHH^{+/-}$ group, and $APOE^{-/-}SAHH^{+/-}$ + mdivi-1(i.p.) group (Fig. 7A). Upon being fed a western diet for 8 weeks, $APOE^{-/-}SAHH^{+/-}$ mice showed increased plasma SAH levels (Fig. 7B) and decreased SAM/SAH ratio (Fig. 7C). There were no significant differences in TG, TC and HDL-C among groups (Supplementary Fig. 6B). The positive area for β-gal staining and oil red staining in the aorta of $APOE^{-/-}SAHH^{+/-}$ mice increased by 4.76 times and 2.97 times, respectively, compared with $APOE^{-/-}$ littermates (Fig. 7D–F). Additionally, we observed a 2.44-time increase in lesion area in the aortic sinus of $APOE^{-/-}SAHH^{+/-}$ mice in comparison with $APOE^{-/-}$ mice (Fig. 7G). However, mdivi-1 treatment reduced the positive area for β-gal staining and oil red staining by 76.3% and 70.5%, respectively in $APOE^{-/-}SAHH^{+/-}$ mice (Fig. 7D–F). A decline of 49.1% in lesion area of aortic sinus was observed as well (Fig. 7G).

3.6. SAHH inhibition induces hypomethylation of the DRP1 promoter and upregulates Drp1 via inhibition of DNMT1

Considering that inhibition of SAHH regulates methylation negatively in organisms, as well as the indication of WGBS, we performed bisulfite-amplicon sequencing targeting the promoter region of the *DRP1* gene in HUVECs treated with ADA or *SAHH* siRNA and observed a decrease in methylation levels in both treatment groups compared to controls (Fig. 8A). Hypomethylation of the promoter region is known to be associated with transcriptional activation, which was confirmed by a luciferase reporter assay that showed an increase in *DRP1* promoter activity by 68.5% and 59.1% in ADA- and *SAHH*-siRNA-treated HUVECs, respectively (Fig. 8B). To further examine the role of CpG methylation in the upregulation of Drp1, methylated *DRP1* promoter plasmid was conducted *in vitro* using Sss1 enzyme and transfected into HUVECs. Interestingly, *in vitro* methylation decreased the activity of the *DRP1* promoter by 36.4% and 55.5% in ADA- and *SAHH*-siRNA-treated HUVECs, respectively (Fig. 8B). DNA transmethylation is catalyzed by DNA methyltransferases (DNMTs) including DNMT1, DNMT3A, and DNMT3B. DNMT1 is responsible for maintaining the methylation status, whereas DNMT3A and DNMT3B are involved in de novo synthesis. After SAHH inhibition, DNMT1 was decreased at both the protein and mRNA levels in HUVECs, while no significant differences were observed in DNMT3A and DNMT3B compared with the control group (Fig. 8C and Supplementary Fig. 7). To further confirm the role of DNMT1 in regulating Drp1 expression, we constructed an adenovirus expressing human DNMT1 and infected HUVECs with it. As expected, overexpression of DNMT1 abolished the increase in promoter activity and protein expression of Drp1 in HUVECs treated with ADA or *SAHH* siRNA (Fig. 8D–E).

4. Discussion

In this study, we identified a new mechanism that links SAHH inhibition to the development of atherosclerosis through vascular senescence. Our results indicate that inhibition of SAHH leads to downregulation of DNMT1 expression, which subsequently reduces methylation over the promoter region of the *DRP1* gene in endothelial cells. This effect leads to imbalanced mitochondrial dynamics and increased mtROS production, ultimately resulting in vascular senescence and atherosclerosis. These findings suggest that SAHH could be a potential target for preventing vascular senescence and atherosclerosis, which are highly prevalent in the elderly population. The inhibition of SAHH has been observed to exert a pro-atherosclerotic effect via epigenetic regulation. Specifically, SAHH inhibition has been shown to induce endothelial inflammation by downregulating H3K27me3 through EZH2 pathway [21], promote oxidative stress in endothelial cells, and impair endothelium-dependent vasodilation via upregulation

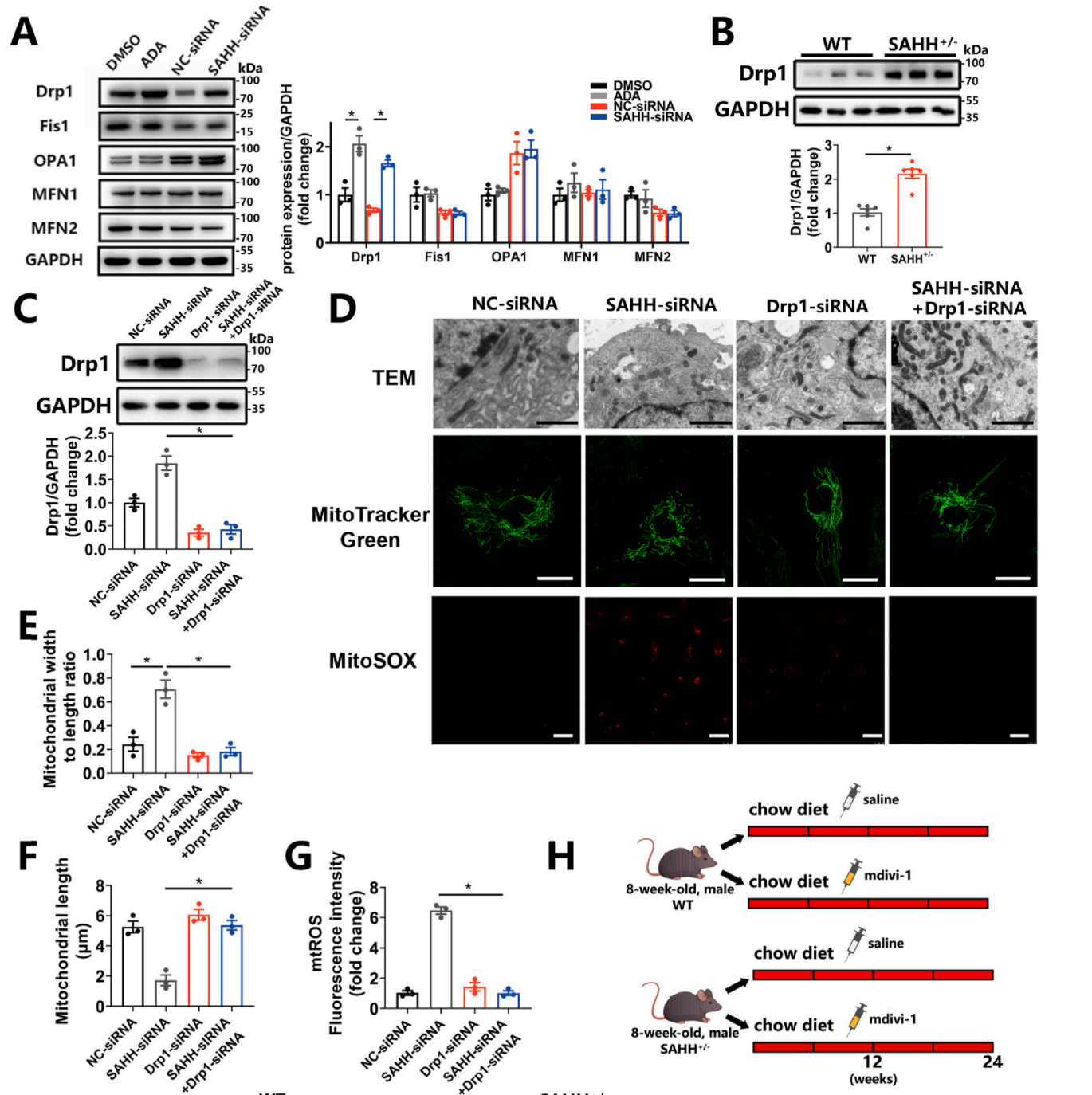

(caption on next page)

Fig. 4. Enhanced mitochondrial fission and mtROS are mediated by Drp1.
HUVECs were treated with ADA (30 μM) or transfected with *SAHH* siRNA for 48 h. 8-week-old *SAHH*$^{+/-}$ mice and wild type littermates were fed a chow diet for 24 weeks (n = 6). **(A)** Western blot analysis of genes regulating mitochondrial dynamics in abovementioned HUVECs groups (n = 3). **(B)** Western blot analysis of Drp1 protein expression in the aorta of abovementioned mouse groups (n = 6). HUVECs were transfected with *DRP1*-siRNA in the presence of ADA or *SAHH*-siRNA. **(C)** Western blot analysis of Drp1 protein expression in abovementioned HUVECs groups (n = 3). **(D)** Morphology of mitochondria detected by transmission electron microscopy, morphological staining of mitochondria using MitoTracker Green dye, and mtROS staininig using MitoSOX dye in abovementioned HUVECs groups (n = 3). Scale bar = 2 μm, 25 μm, and 25 μm (top to bottom). **(E)** Quantification of the ratio of mitochondrial width to length according to TEM examination in **(D)**. **(F)** Quantification of the mitochondrial length according to MitoTracker Green staining in **(D)**. **(G)** Quantification of mtROS levels according to MitoSOX staining in **(D)**. **(H)** Male *SAHH*$^{+/-}$ mice and their wild type littermates were divided into 4 groups (n = 6): wild type group, wild type + mdivi-1 (i.p. 10 mg/kg twice a week) group, *SAHH*$^{+/-}$ group, and *SAHH*$^{+/-}$ + mdivi-1 (i.p. 10 mg/kg twice a week) group and fed a chow diet from 8 to 32 weeks of age. **(I)** Morphology of mitochondria in the aortic endothelium detected by transmission electron microscopy and DHE staining of the aorta in abovementioned mouse groups (n = 6). Scale bar = 2 μm and 250 μm (top to bottom). **(J)** Quantification of the ratio of mitochondrial width to length according to TEM examination in **(I)**. **(K)** Quantification of DHE fluorescence density according to DHE staining in **(I)**. For all bar graphs, data are means ± SEM, $*p < 0.05$ (determined by the *t*-test or 1-way ANOVA). (For interpretation of the references to colour in this figure legend, the reader is referred to the Web version of this article.)

of p66shc [20]. Given that vascular senescence is linked with epigenetics modifications and contributes to atherosclerosis [22], we hypothesized that SAHH inhibition might induce vascular senescence and thereby accelerate the development of atherosclerosis. We first identified an association between vascular aging and plasma SAH levels in our case-control study. Subsequently, we confirmed that SAHH inhibition affects vascular senescence using the *SAHH*$^{+/-}$ knockout mice model. Notably, the pro-senescence effect of SAHH inhibition was mainly observed in the endothelial layer, which is further verified using HUVECs models treated with ADA and *SAHH* siRNA. One possible explanation for this selective effect is the pivotal role of the endothelium in cardiovascular pathogenesis. Alteration of the endothelium is reported to be the initial step in cardiovascular diseases and may be seen in their early phase [22]. Risk factors such as hypercholesterolemia, hypertension, diabetes, and smoking, for example, are associated with endothelial dysfunction, which in turn contributes to arterial stiffness, atherosclerosis, stroke, and coronary artery disease [23].

As an essential component of the methionine cycle, SAH metabolism has been tightly linked to cellular senescence and aging in organisms. For example, the activity of SAHH decreases and SAH levels increase with the aging of bone marrow mesenchymal stem cells [24] and red blood cells [25]. Age-dependent accumulation of SAH was also found *in vivo* in Drosophilas [26] and rats [27]. In humans, the SAH levels of cerebrospinal fluid manifested an age-dependent increase [28]. Additionally, SAH accumulation has been proposed to be associated with age-related cognitive diseases [29]. Today, in an increasingly aging society, the demand for the prevention of age-related diseases increases further. Our findings might provide new insight into potential therapies for age-associated diseases, such as Alzheimer's disease, diabetes, and cancer, as SAHH inhibition regulates cellular senescence in addition to affecting atherosclerosis.

Mitochondria are organelles with highly dynamic structures maintained by a delicate equilibrium between fission and fusion processes [8]. In mammalian cells, mitochondrial fission is regulated by Drp1 and Fis1, while MFN1&2 and OPA1 participate in the fusion process [10]. Perturbation of mitochondrial dynamics can lead to cellular senescence. For instance, myocardial senescence induced by hypoxia in rats depends on Drp1-mediated mitochondrial fission [30]. Protein disulfide isomerase inhibits Drp1-mediated mitochondrial fission, thereby limiting endothelial senescence [31]. In fungi and *C. elegans*, inhibiting mitochondrial fission by knocking down Drp1 expands the lifespan [12,32]. In line with these findings, WGBS in the current study indicated that differentially methylated genes between the SAHH inhibition and control groups were enriched in terms related to mitochondrial dynamics. We further confirmed the fission-prone changes of mitochondria in *SAHH*$^{+/-}$ mice and HUVECs by TEM and specific fluorescence staining. Our loss-of-function experiments demonstrated that Drp1 mediates the effect of SAHH inhibition on mitochondrial fission and subsequent endothelial senescence both *in vitro* and *in vivo*.

Abnormal shape of mitochondria can cause a series of pathological changes, including inefficient oxidative phosphorylation, ATP depletion, and increased levels of mitochondria-derived ROS (mtROS) [8]. Mounting evidence suggests that mtROS play a critical role in the link between aberrant mitochondrial dynamics and cellular senescence in various cell types, including T cells, hepatocellular carcinoma cells, microglia, and endothelial cells [31,33–35]. Herein, elevated mtROS was observed in HUVECs with SAHH inhibition. Enhanced ROS levels were also detected in the aorta of *SAHH*$^{+/-}$ mice. To investigate the role of mtROS in vascular senescence induced by SAHH inhibition, we used mitoTEMPO, a specific quencher that targets mtROS. Our results showed that the senescence phenotypes of HUVECs were attenuated after mitoTEMPO treatment. *In vivo*, ameliorated vascular senescence were also observed in *SAHH*$^{+/-}$ mice injected with mitoTEMPO compared with the control. To determine the origin of the elevated mtROS, we downregulated Drp1 *in vitro* and *in vivo*. The results indicated that the elevated mtROS functioned downstream of the enhanced Drp1-mediated mitochondrial fragmentation without a feedback effect. Mitochondrial fission may also be induced by mitochondrial dysfunction in order to segregate and degrade the damaged portion through mitophagy. Mitophagy is a vital process responsible for selective removal of excess or damaged mitochondrial through autophagy and plays a role in mitochondrial homeostasis alongside mitochondrial dynamics. Growing evidence suggests that dysregulated mitophagy contributes to vascular senescence by promoting the accumulation of damaged mitochondria and ROS [36,37]. Conversely, the upregulation of mitophagy, such as through trehalose treatment, has been shown to reduce superoxide and reverse several phenotypic manifestations of vascular aging in aged mice [38]. In light of these findings, we sought to investigate the role of mitophagy in HUVECs under SAHH inhibition and observed an increase in mitophagy in the SAHH inhibition group compared to the control. This finding can be attributed to the disruption of mitochondrial dynamics, which is known to promote intracellular mitophagy. Specifically, previous studies have demonstrated that Drp1-mediated mitochondrial fission is a prerequisite for mitophagy in yeast [39]. In mouse heart and brain, parkin-independent mitophagy is also induced by Drp1-mediated mitochondrial fission [40]. Additionally, the depletion of Cav-1 in breast cancer cells enhances both mitochondrial fusion and fission, and thereby facilitating mitophagy [41]. However, we acknowledge that further investigations are required in the future to determine whether SAHH inhibition directly affects mitophagy.

MtROS has been reported to elicit both cellular senescence and apoptosis [42]. To investigate the effect of herein SAHH model on apoptosis, we examined the occurrence of apoptosis in HUVECs and observed no significant difference between the SAHH group and the control group. It is possible that the intensity of mtROS induced by SAHH inhibition was not sufficient to trigger apoptosis. Oxidative stress elicits downstream cellular events in a dose-response manner. For instance, high doses of H_2O_2 can cause overwhelming stress and lead to apoptosis, while lower doses of H_2O_2 induce less severe damage and cellular senescence in F65 and IMR90 human diploid fibroblasts [43,44]. Furthermore, the quaternary structure, post-translational

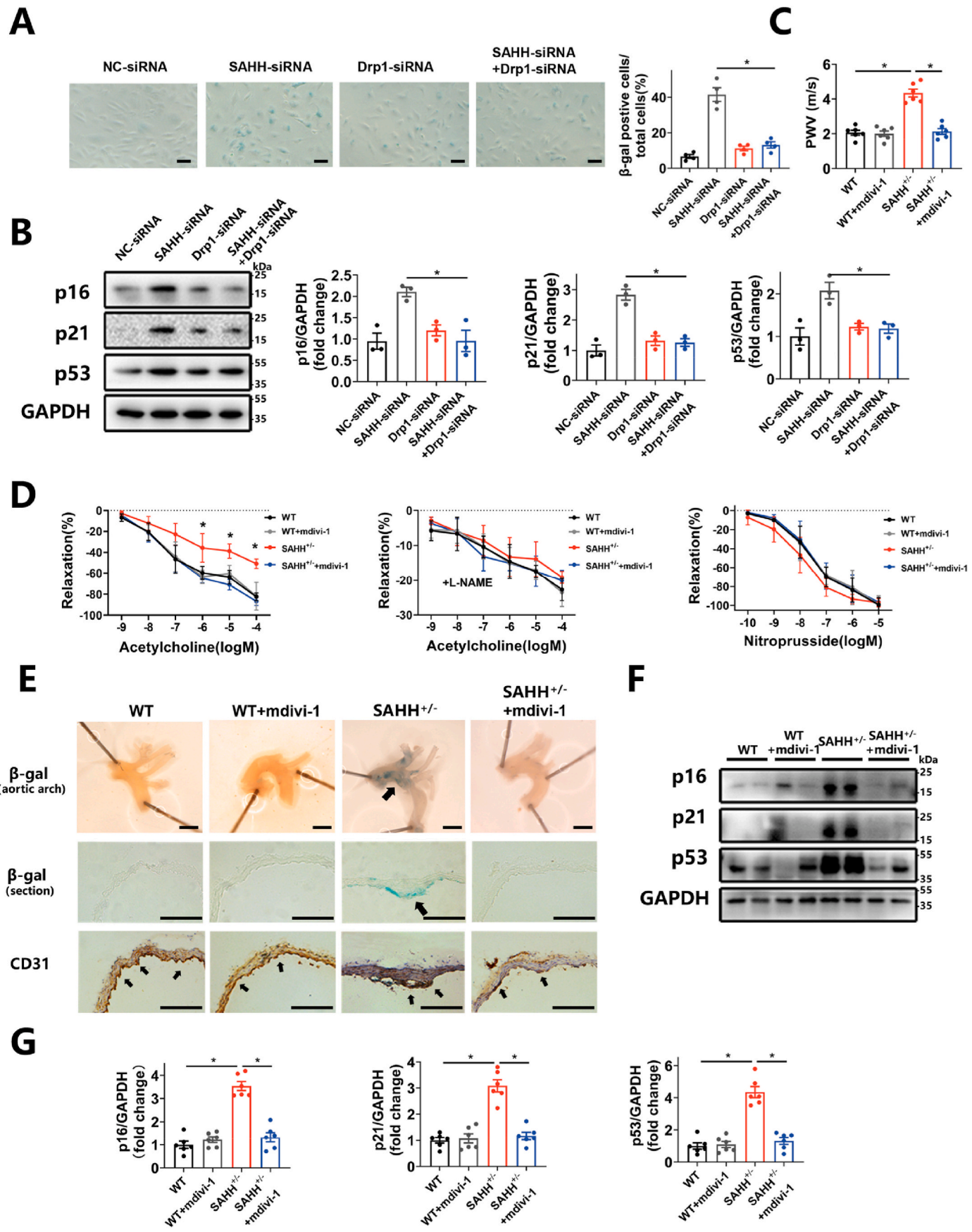

(caption on next page)

Fig. 5. Drp1 inhibition rescues the endothelial senescence and vascular senescence induced by SAHH inhibition.
HUVECs were transfected with *DRP1*-siRNA in the presence of *SAHH*-siRNA. Male $SAHH^{+/-}$ mice and their wild type littermates were divided into 4 groups (n = 6): wild type group, wild type + mdivi-1 (i.p. 10 mg/kg twice a week) group, $SAHH^{+/-}$ group, and $SAHH^{+/-}$ + mdivi-1 (i.p. 10 mg/kg twice a week) group and fed a chow diet from 8 to 32 weeks of age. **(A)** SA β-gal staining of HUVECs from the abovementioned 4 groups (n = 4). Scale bar = 200 μm. **(B)** Western blot analysis of p16, p21, and p53 protein expression in HUVECs from the abovementioned 4 groups (n = 3). **(C)** Aortic pulse wave velocity of mice from the abovementioned mouse groups (n = 6). **(D)** Endothelium-dependent vascular relaxation in response to acetylcholine in the presence or absence of eNOS inhibitor L-NAME, and endothelium-independent vascular relaxation in response to nitroprusside in abovementioned mouse groups (n = 6). **(E)** SA β-gal staining and CD31 immunohistochemical staining of the aortic arch of the abovementioned mouse groups (n = 6). Scale bar = 2 mm, 250 μm, and 250 μm (from the top to bottom). **(F)–(G)** Western blot analysis of p16, p21, and p53 protein expression in mouse aorta from the abovementioned mouse groups (n = 6). SA β-gal, senescence-associated β-galactosidase; PWV, pulse wave velocity. For all bar graphs, data are means ± SEM, $^*p < 0.05$ (determined by the 1-way ANOVA).

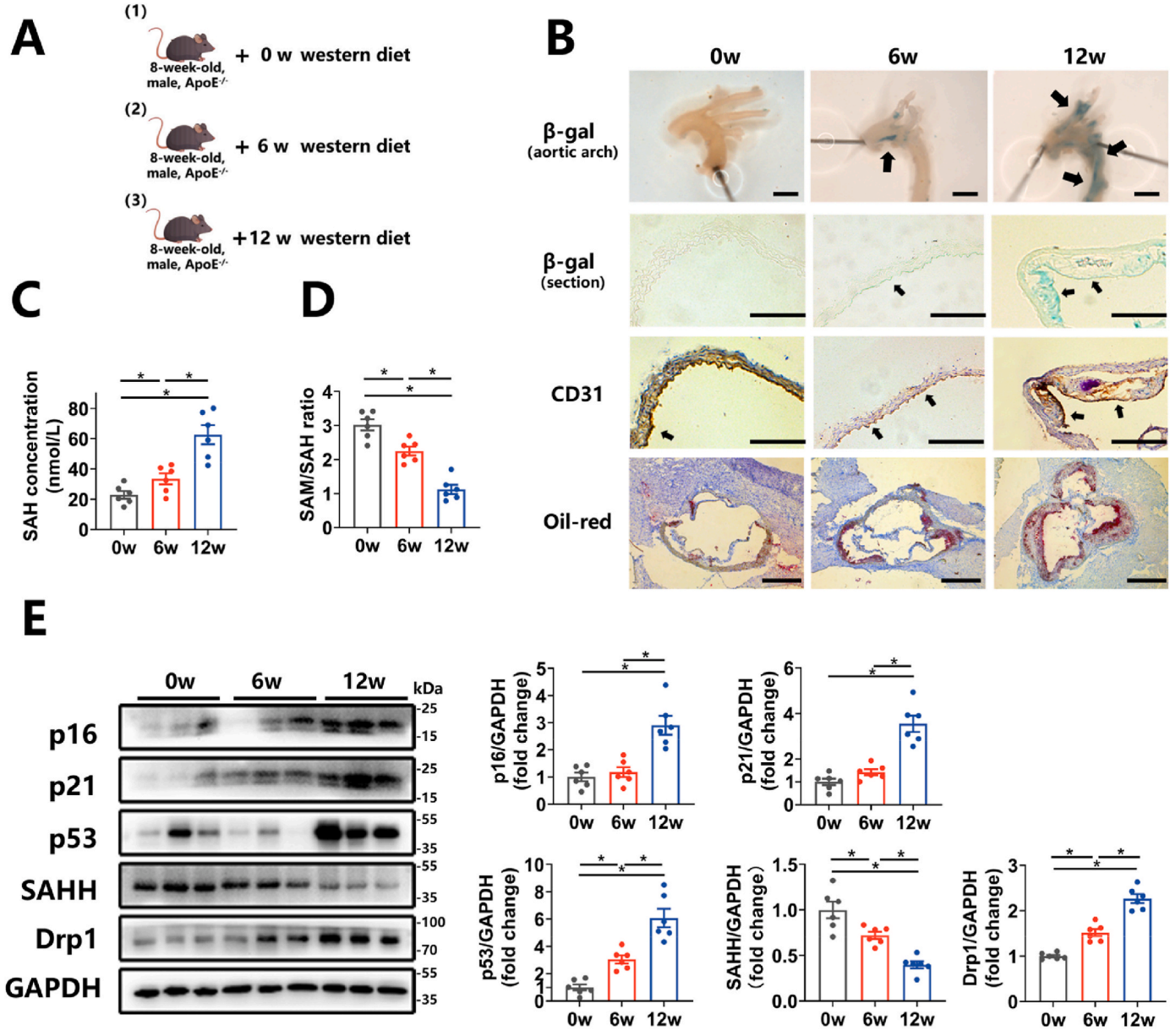

Fig. 6. SAHH declines and vascular senescence increases during the progression of atherosclerosis in $ApoE^{-/-}$ mice.
(A) 8-week-old male $APOE^{-/-}$ mice were divided into 3 groups (n = 6) and fed a western diet for 0, 6 and 12 weeks, respectively. **(B)** SA β-gal staining and CD31 immunohistochemical staining of the aortic arch and oil red O staining of the aortic sinus of the abovementioned mice (n = 6). Scale bar = 2 mm, 250 μm, 250 μm, and 500 μm (from the top to bottom). **(C)–(D)** Plasma concentrations of SAH and the SAM/SAH ratios in the abovementioned mice (n = 6). Plasma levels of SAH and SAM were measured by stable-isotope dilution liquid chromatography–electrospray tandem mass spectrometry. **(E)** Western blot analysis of p16, p21, p53, SAHH, and Drp1 protein expression in the aorta of the abovementioned mice (n = 6). SA β-gal, senescence-associated β-galactosidase. For all bar graphs, data are means ± SEM, $^*p < 0.05$ (determined by the 1-way ANOVA). (For interpretation of the references to colour in this figure legend, the reader is referred to the Web version of this article.)

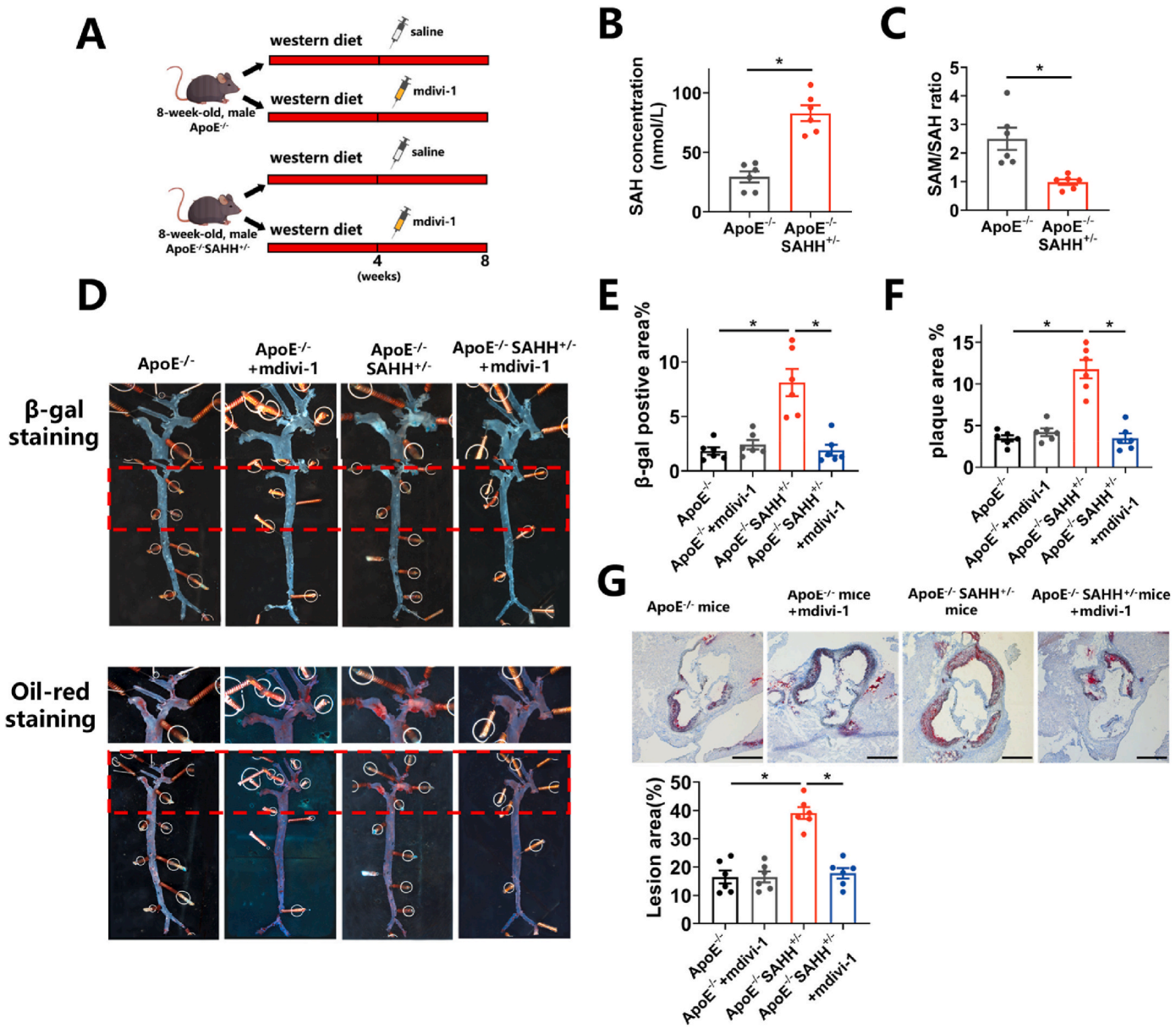

Fig. 7. SAHH inhibition accelerates atherosclerosis in a Drp1-dependent pathway.
(A) 8-week-old male $APOE^{-/-}SAHH^{+/-}$ mice and $APOE^{-/-}$ littermates were divided into 4 groups (n = 6): $APOE^{-/-}$group, $APOE^{-/-}$ + mdivi-1 (i.p. 10 mg/ml twice a week) group, $APOE^{-/-}SAHH^{+/-}$ group, and $APOE^{-/-}SAHH^{+/-}$ + mdivi-1 (i.p. 10 mg/ml twice a week) group and fed a western diet from 8 to 16 weeks of age. **(B)–(C)** Plasma concentrations of SAH and the SAM/SAH ratios in the abovementioned mice (n = 6). Plasma levels of SAH and SAM were measured by stable-isotope dilution liquid chromatography–electrospray tandem mass spectrometry. **(D)** Representative SA β-gal staining images and oil red O staining images of the same aorta in abovementioned mouse groups (n = 6). **(E)–(F)** Quantification of the SA β-gal staining and oil red O staining areas in **(D)**. **(G)** Oil red O staining of aortic sinus sections in the abovementioned mouse groups (n = 6). Scale bar = 500 μm. SA β-gal, senescence-associated β-galactosidase. For all bar graphs, data are means ± SEM, *$p < 0.05$ (determined by the 1-way ANOVA). (For interpretation of the references to colour in this figure legend, the reader is referred to the Web version of this article.)

modification, and kinetic expression of p53 can influence whether cells undergo apoptosis or senescence [45]. These factors were not explored in our study and warrant further work in the future, as well as other signaling pathways such as PTEN/PI3K/AKT, that regulate both apoptosis and senescence.

Drp1 is a GTPase belonging to dynamin superfamily and regulates mitochondrial fission. Drp1 can be modified by phosphorylation, ubiquitylation, SUMOylation, and S-nitrosylation [46]. In addition, epigenetic modifications, such as methylation, have been shown to participate in Drp1 regulation in recent years. For example, proteins associated with obesity in fat mass have been shown to impair Drp1-mediated mitochondrial fission by decreasing m6A methylation in *DRP1* mRNA [47]. In the HUVEC model of SAHH inhibition, we observed decreased methylation occupancy over the promoter region and decreased promoter activity of the *DRP1* gene, concomitant with downregulation of DNMT1, an enzyme responsible for DNA methylation maintenance. An *in vitro* methylation assay confirmed that the methylated promoter could abrogate Drp1 upregulation in HUVECs with SAHH inhibition. In line with it, further overexpression of DNMT1 reduced Drp1 expression in HUVECs treated with SAHH inhibition. Our investigation provided evidence that DNA methylation participated in Drp1 regulation. Consistent with our findings, a study on BeWo cells treated with polybrominated diphenyl ethers reported increased Drp1 expression and hypomethylation of the promoter region of *DRP1,* but the

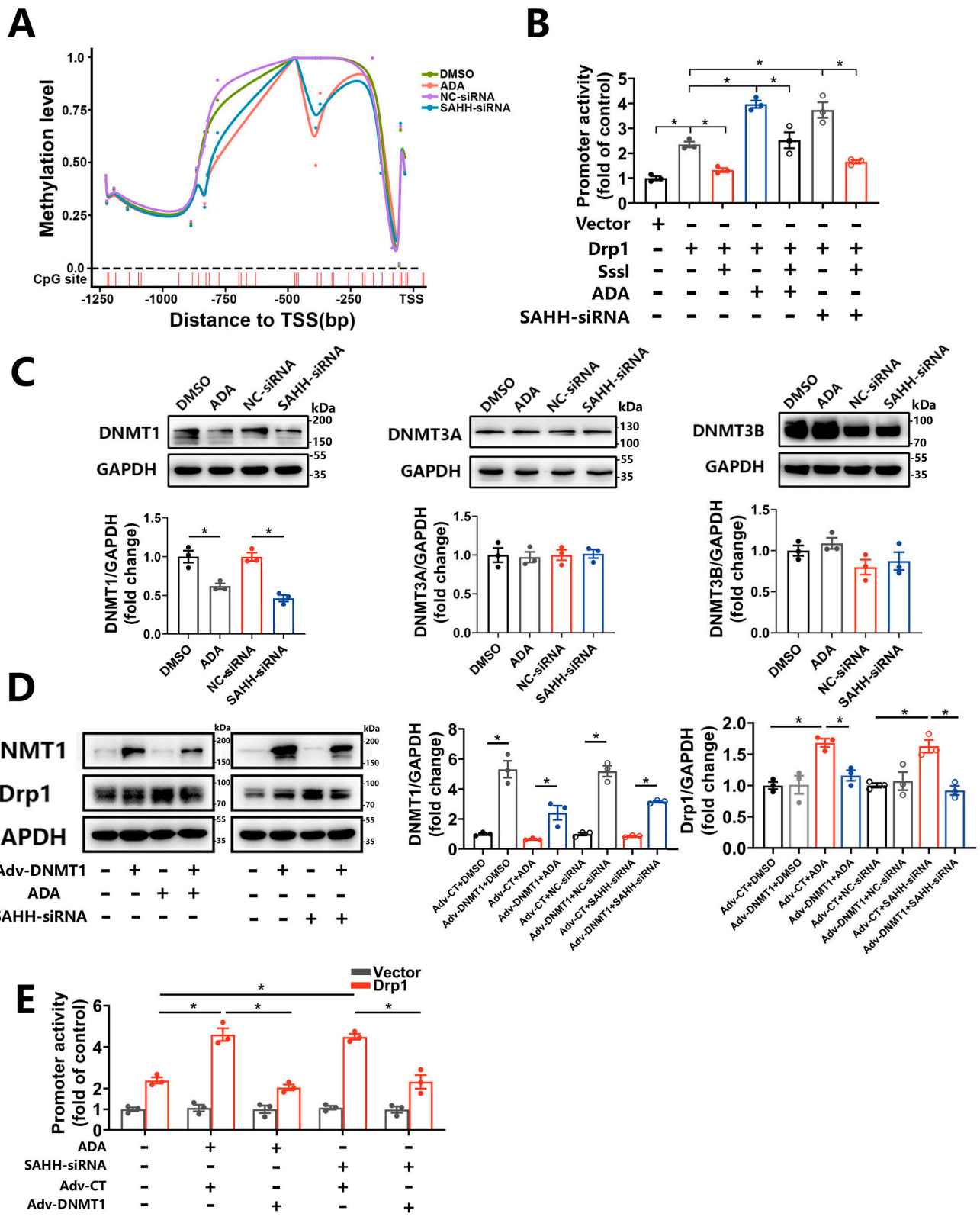

Fig. 8. SAHH inhibition induces hypomethylation of the *DRP* promoter and upregulation of Drp1 via inhibition of DNMT1.
(A) The methylation level of GpG sites over the promoter region of the *DRP1* gene in HUVECs treated with ADA (30 μM) or transfected with *SAHH* siRNA for 48 h by BA-seq. **(B)** HUVECs transfected with unmethylated or methylated *DRP1* promoter by the CpG methylase Sss1 were treated with ADA (30 μM) or transfected with *SAHH* siRNA for 48 h. *DRP1* promoter activity in abovementioned HUVECs measured using a luciferase reporter kit (n = 3). **(C)** Western blot analysis of DNMT1, DNMT3A, and DNMT3B in HUVECs treated with ADA (30 μM) or transfected with *SAHH* siRNA for 48 h (n = 3). **(D)** Western blot analysis of DNMT1 and Drp1 in HUVECs overexpressing DNMT1 in the presence of ADA and *SAHH*-siRNA (n = 3). **(E)** HUVECs transfected with the *DRP1* promoter or control plasmid were infected with Adv-CT or Adv-DNMT1 for 24 h and then treated with ADA (30 μM) or *SAHH* siRNA for another 24 h. *DRP1* promoter activity measured by a luciferase reporter kit in abovementioned HUVECs groups (n = 3). TSS, transcription start site; BA-seq, amplicon bisulfite sequencing. For all bar graphs, data are means ± SEM, *$p <$ 0.05 (determined by the *t*-test or 1-way ANOVA).

mechanism was not further investigated [48]. In addition, our data confirmed the critical role of DNMT1 in the regulation of Drp1. Intriguingly, DNMT1 deficiency has been reported to lead to hypomethylation of the *DRP1* gene and promoted the aberrant binding of CTCF, inhibiting Drp1-mediated mitochondrial fission in adipocytes [49]. The discrepancy could be explained by the fact that although DNA methylation has been generally recognized as a repressor of transcription by inhibiting the binding between transcription factors and promoter regions, it can also participate in transcriptional activation [50]. Furthermore, the interplay between *cis*-transcription factors and the promoter region was not explored in that study and warrants further investigation, which was mentioned as a limitation by the authors [49].

However, our study is subject to several limitations that necessitate further investigation. Firstly, we only reported an association between vascular aging and SAHH inhibition at the population level, without further mechanistic confirmation. Secondly, we did not discuss the potential effects of SAHH inhibition on other cell types within vasculature, such as smooth muscle cells and macrophages. Thirdly, the utilization of a whole-body knockout mouse model prevents us from completely excluding indirect effects of other tissues on the vasculature, highlighting the need for future research employing endothelium-specific knockout mouse models. Lastly, we have not conducted experiments involving further over-expression or upregulation of SAHH in the current study.

In summary, we demonstrate that inhibition of SAHH results in vascular senescence and accelerates atherosclerosis through epigenetic regulation of Drp1-mediated mitochondrial fission. Our findings suggest that SAHH inhibition and SAH elevation can serve as hallmark indicators of vascular senescence and atherosclerosis, and may provide insights into prevention and therapies for these conditions.

Funding

This work was supported and funded by the National Natural Science Foundation of China (Grant No. U22A20360), the State Key Program of National Natural Science Foundation of China (Grant No. 81730090), and the National Key R&D Program of China (SQ2019YFC1604603).

Author contribution statement

Conceptualization, Yiran You and Wenhua Ling; Methodology, Yiran You, Xu Chen, and Qian Chen; Investigation, Yiran You and Yu Chen; Writing – Original Draft, Yiran You; Writing – Review & Editing, Juan Pang; Funding Acquisition, Wenhua Ling; Resources, Qiannan Liu, Yupeng Zeng, Jiaxin Mi, and Yi Tang; Project administration, Hongliang Xue and Jinghe Xiao.

Data availability statements

The data underlying this article will be shared on reasonable request to the corresponding author.

Declaration of competing interest

The authors declare no conflict of interest.

Appendix A. Supplementary data

Supplementary data to this article can be found online at https://doi.org/10.1016/j.redox.2023.102828.

References

[1] M. Rafieian-Kopaei, M. Setorki, M. Doudi, A. Baradaran, H. Nasri, Atherosclerosis: process, indicators, risk factors and new hopes, Int. J. Prev. Med. 5 (2014) 927–946.

[2] J.C. Wang, M. Bennett, Aging and atherosclerosis mechanisms, functional consequences, and potential therapeutics for cellular senescence, Circ. Res. 111 (2012) 245–259, https://doi.org/10.1161/circresaha.111.261388.

[3] B.G. Childs, D.J. Baker, T. Wijshake, C.A. Conover, J. Campisi, J.M. van Deursen, Senescent intimal foam cells are deleterious at all stages of atherosclerosis, Science 354 (2016) 472–477, https://doi.org/10.1126/science.aaf6659.

[4] G. Yang, Y. Lei, A. Inoue, L. Piao, L. Hu, H. Jiang, T. Sasaki, H. Wu, W. Xu, C. Yu, et al., Exenatide mitigated diet-induced vascular aging and atherosclerotic plaque growth in ApoE-deficient mice under chronic stress, Atherosclerosis 264 (2017) 1–10, https://doi.org/10.1016/j.atherosclerosis.2017.07.014.

[5] G.H. Lee, T.H. Hoang, E.S. Jung, S.J. Jung, S.K. Han, M.J. Chung, S.W. Chae, H. J. Chae, Anthocyanins attenuate endothelial dysfunction through regulation of uncoupling of nitric oxide synthase in aged rats, Aging Cell 19 (2020), e13279, https://doi.org/10.1111/acel.13279.

[6] C. Sun, S. Fan, X. Wang, J. Lu, Z. Zhang, D. Wu, Q. Shan, Y. Zheng, Purple sweet potato color inhibits endothelial premature senescence by blocking the NLRP3 inflammasome, J. Nutr. Biochem. 26 (2015) 1029–1040, https://doi.org/10.1016/j.jnutbio.2015.04.012.

[7] J. Jin, Y.F. Liu, L.H. Huang, H. Tan, Advances in epigenetic regulation of vascular aging, Rev. Cardiovasc. Med. 20 (2019) 19–25, https://doi.org/10.31083/j.rcm.2019.01.3189.

[8] J. Jezek, K.F. Cooper, R. Strich, Reactive oxygen species and mitochondrial dynamics: the yin and yang of mitochondrial dysfunction and cancer progression, ARTN 13, Antioxidants-Basel 7 (2018), https://doi.org/10.3390/antiox7010013.

[9] Y. Uchikado, Y. Ikeda, M. Ohishi, Current understanding of the pivotal role of mitochondrial dynamics in cardiovascular diseases and senescence, Frontiers in cardiovascular medicine 9 (2022), 905072, https://doi.org/10.3389/fcvm.2022.905072.

[10] D.V. Ziegler, C.D. Wiley, M.C. Velarde, Mitochondrial effectors of cellular senescence: beyond the free radical theory of aging, Aging Cell 14 (2015) 1–7, https://doi.org/10.1111/acel.12287.

[11] A.K. Biala, R. Dhingra, L.A. Kirshenbaum, Mitochondrial dynamics: orchestrating the journey to advanced age, J. Mol. Cell. Cardiol. 83 (2015) 37–43, https://doi.org/10.1016/j.yjmcc.2015.04.015.

[12] S.N. Chaudhari, E.T. Kipreos, Increased mitochondrial fusion allows the survival of older animals in diverse C. elegans longevity pathways, ARTN 182, Nat. Commun. 8 (2017), https://doi.org/10.1038/s41467-017-00274-4.

[13] D. Ma, B. Zheng, H.L. Liu, Y.B. Zhao, X. Liu, X.H. Zhang, Q. Li, W.B. Shi, T. Suzuki, J.K. Wen, Klf5 down-regulation induces vascular senescence through eIF5a depletion and mitochondrial fission, PLoS Biol. 18 (2020), e3000808, https://doi.org/10.1371/journal.pbio.3000808.

[14] P. Vizan, L. Di Croce, S. Aranda, Functional and pathological roles of AHCY, Front. Cell Dev. Biol. 9 (2021), 654344, https://doi.org/10.3389/fcell.2021.654344.

[15] H.P. Zhang, Z.H. Liu, S.C. Ma, H. Zhang, F.Q. Kong, Y.Y. He, X.L. Yang, Y.H. Wang, H. Xu, A.N. Yang, et al., Ratio of S-adenosylmethionine to S-adenosylhomocysteine as a sensitive indicator of atherosclerosis, Mol. Med. Rep. 14 (2016) 289–300, https://doi.org/10.3892/mmr.2016.5230.

[16] Y. Xiao, Y. Zhang, M. Wang, X. Li, D. Su, J. Qiu, D. Li, Y. Yang, M. Xia, W. Ling, Plasma S-adenosylhomocysteine is associated with the risk of cardiovascular events in patients undergoing coronary angiography: a cohort study, Am. J. Clin. Nutr. 98 (2013) 1162–1169, https://doi.org/10.3945/ajcn.113.058727.

[17] X. Luo, Y. Xiao, F. Song, Y. Yang, M. Xia, W. Ling, Increased plasma S-adenosylhomocysteine levels induce the proliferation and migration of VSMCs through an oxidative stress-ERK1/2 pathway in apoE(-/-) mice, Cardiovasc. Res. 95 (2012) 241–250, https://doi.org/10.1093/cvr/cvs130.

[18] Y. Xiao, W. Huang, J. Zhang, C. Peng, M. Xia, W. Ling, Increased plasma S-adenosylhomocysteine-accelerated atherosclerosis is associated with epigenetic regulation of endoplasmic reticulum stress in apoE-/- mice, Arterioscler. Thromb. Vasc. Biol. 35 (2015) 60–70, https://doi.org/10.1161/atvbaha.114.303817.

[19] Y.R. You, X.Y. Sun, J.H. Xiao, Y. Chen, X. Chen, J. Pang, J.X. Mi, Y. Tang, Q.N. Liu, W.H. Ling, Inhibition of S-adenosylhomocysteine hydrolase induces endothelial senescence via hTERT downregulation, Atherosclerosis 353 (2022) 1–10, https://doi.org/10.1016/j.atherosclerosis.2022.06.002.

[20] Y. Xiao, J. Xia, J. Cheng, H. Huang, Y. Zhou, X. Yang, X. Su, Y. Ke, W. Ling, Inhibition of S-adenosylhomocysteine hydrolase induces endothelial dysfunction via epigenetic regulation of p66shc-mediated oxidative stress pathway, Circulation 139 (2019) 2260–2277, https://doi.org/10.1161/circulationaha.118.036336.

[21] M. Barroso, D. Kao, H.J. Blom, I. Tavares de Almeida, R. Castro, J. Loscalzo, D. E. Handy, S-adenosylhomocysteine induces inflammation through NFkB: a possible role for EZH2 in endothelial cell activation, Biochim. Biophys. Acta 1862 (2016) 82–92, https://doi.org/10.1016/j.bbadis.2015.10.019.

[22] G.H. Jia, A.R. Aroor, C. Jia, J.R. Sowers, Endothelial cell senescence in aging-related vascular dysfunction, Biochim. Biophys. Acta, Mol. Basis Dis. 1865 (2019) 1802–1809, https://doi.org/10.1016/j.bbadis.2018.08.008.

[23] G.H. Jia, A.R. Aroor, V.G. DeMarco, L.A. Martinez-Lemus, G.A. Meininger, J. R. Sowers, Vascular stiffness in insulin resistance and obesity, Front. Physiol. 6 (2015) 231, https://doi.org/10.3389/fphys.2015.00231.

[24] Y. Wang, Y. Zhang, K. Chen, J. Liu, D. Wu, Y. Cheng, H. Wang, Y. Li, Insufficient S-adenosylhomocysteine hydrolase compromises the beneficial effect of diabetic BMSCs on diabetic cardiomyopathy, Stem Cell Res. Ther. 13 (2022) 418, https://doi.org/10.1186/s13287-022-03099-1.

[25] A. Bozzi, B. Furciniti-La Chiusa, R. Strom, C. Crifò, S-adenosylhomocysteine hydrolase and adenosine deaminase activities in human red cell ageing, Clinica chimica acta; international journal of clinical chemistry 189 (1990) 81–86, https://doi.org/10.1016/0009-8981(90)90237-m.

[26] A.A. Parkhitko, R. Binari, N. Zhang, J.M. Asara, F. Demontis, N. Perrimon, Tissue-specific down-regulation of S-adenosyl-homocysteine via suppression of dAhcyL1/dAhcyL2 extends health span and life span in Drosophila, Genes & development 30 (2016) 1409–1422, https://doi.org/10.1101/gad.282277.116.

[27] G. Varela-Moreiras, L. Pérez-Olleros, M. García-Cuevas, B. Ruiz-Roso, Effects of ageing on folate metabolism in rats fed a long-term folate deficient diet. International journal for vitamin and nutrition research. Internationale Zeitschrift Fur Vitamin- und Ernahrungsforschung, J. Int. Vitaminol. Nutr. 64 (1994) 294–299.

[28] D.E. Smith, Y.M. Smulders, H.J. Blom, J. Popp, F. Jessen, A. Semmler, M. Farkas, M. Linnebank, Determinants of the essential one-carbon metabolism metabolites, homocysteine, S-adenosylmethionine, S-adenosylhomocysteine and folate, in cerebrospinal fluid, Clin. Chem. Lab. Med. 50 (2012) 1641–1647, https://doi.org/10.1515/cclm-2012-0056.

[29] B.P. Kennedy, T. Bottiglieri, E. Arning, M.G. Ziegler, L.A. Hansen, E. Masliah, Elevated S-adenosylhomocysteine in Alzheimer brain: influence on methyltransferases and cognitive function, J. Neural. Transm. 111 (2004) 547–567, https://doi.org/10.1007/s00702-003-0096-5.

[30] A. Nishimura, T. Shimauchi, T. Tanaka, K. Shimoda, T. Toyama, N. Kitajima, T. Ishikawa, N. Shindo, T. Numaga-Tomita, S. Yasuda, et al., Hypoxia-induced interaction of filamin with Drp1 causes mitochondrial hyperfission-associated myocardial senescence, Sci. Signal. 11 (2018), https://doi.org/10.1126/scisignal.aat5185. ARTN eaat5185.

[31] Y.M. Kim, S.W. Youn, V. Sudhahar, A. Das, R. Chandhri, H.C. Grajal, J. Kweon, S. Leanhart, L.Y. He, P.T. Toth, et al., Redox regulation of mitochondrial fission protein Drp1 by protein disulfide isomerase limits endothelial senescence, Cell Rep. 23 (2018) 3565–3578, https://doi.org/10.1016/j.celrep.2018.05.054.

[32] C.Q. Scheckhuber, N. Erjavec, A. Tinazli, A. Hamann, T. Nystrom, H.D. Osiewacz, Reducing mitochondrial fission results in increased life span and fitness of two fungal ageing models, Nat. Cell Biol. 9 (2007) 99–U129, https://doi.org/10.1038/ncb1524.

[33] D. Röth, P.H. Krammer, K. Gülow, Dynamin related protein 1-dependent mitochondrial fission regulates oxidative signalling in T cells, FEBS Lett. 588 (2014) 1749–1754, https://doi.org/10.1016/j.febslet.2014.03.029.

[34] Q. Huang, L. Zhan, H. Cao, J. Li, Y. Lyu, X. Guo, J. Zhang, L. Ji, T. Ren, J. An, et al., Increased mitochondrial fission promotes autophagy and hepatocellular carcinoma cell survival through the ROS-modulated coordinated regulation of the NFKB and TP53 pathways, Autophagy 12 (2016) 999–1014, https://doi.org/10.1080/15548627.2016.1166318.

[35] J. Park, J.S. Min, U. Chae, J.Y. Lee, K.S. Song, H.S. Lee, H.J. Lee, S.R. Lee, D.S. Lee, Anti-inflammatory effect of oleuropein on microglia through regulation of Drp1-dependent mitochondrial fission, J. Neuroimmunol. 306 (2017) 46–52, https://doi.org/10.1016/j.jneuroim.2017.02.019.

[36] T.J. LaRocca, G.D. Henson, A. Thorburn, A.L. Sindler, G.L. Pierce, D.R. Seals, Translational evidence that impaired autophagy contributes to arterial ageing, Journal of Physiology-London 590 (2012) 3305–3316, https://doi.org/10.1113/jphysiol.2012.229690.

[37] I. Lee, S. Piao, S. Kim, H. Nagar, S.J. Choi, M. Kim, G.H. Vu, B.H. Jeon, C.S. Kim, IDH2 deficiency promotes endothelial senescence by eliciting miR-34b/c-Mediated suppression of mitophagy and increased ROS production, Antioxidants-Basel 12 (2023) 585, https://doi.org/10.3390/antiox12030585.

[38] T.J. LaRocca, C.M. Hearon, G.D. Henson, D.R. Seals, Mitochondrial quality control and age-associated arterial stiffening, Exp. Gerontol. 58 (2014) 78–82, https://doi.org/10.1016/j.exger.2014.07.008.

[39] F. Nieto-Jacobo, D. Pasch, C.W. Basse, The mitochondrial dnm1-like fission component is required for lga2-induced mitophagy but dispensable for starvation-induced mitophagy in ustilago maydis, Eukaryot. Cell 11 (2012) 1154–1166, https://doi.org/10.1128/ec.00115-12.

[40] Y. Kageyama, M. Hoshijima, K. Seo, D. Bedja, P. Sysa-Shah, S.A. Andrabi, W. Chen, A. Hoke, V.L. Dawson, T.M. Dawson, et al., Parkin-independent mitophagy requires Drp1 and maintains the integrity of mammalian heart and brain, EMBO J. 33 (2014) 2798–2813, https://doi.org/10.15252/embj.201488658.

[41] Y. Jiang, S. Krantz, X. Qin, S. Li, H. Gunasekara, Y.M. Kim, A. Zimnicka, M. Bae, K. Ma, P.T. Toth, et al., Caveolin-1 controls mitochondrial damage and ROS production by regulating fission-fusion dynamics and mitophagy, Redox Biol. 52 (2022), 102304, https://doi.org/10.1016/j.redox.2022.102304.

[42] P. Davalli, T. Mitic, A. Caporali, A. Lauriola, D. D'Arca, ROS, cell senescence, and novel molecular mechanisms in aging and age-related diseases, Oxidative Medicine and Cellular Longevity 2016 (2016), 3565127, https://doi.org/10.1155/2016/3565127.

[43] Q. Chen, B.N. Ames, Senescence-like growth arrest induced by hydrogen peroxide in human diploid fibroblast F65 cells, Proc. Natl. Acad. Sci. U. S. A. 91 (1994) 4130–4134, https://doi.org/10.1073/pnas.91.10.4130.

[44] Q.M. Chen, J.P. Liu, J.B. Merrett, Apoptosis or senescence-like growth arrest: influence of cell-cycle position, p53, p21 and bar in H2O2 response of normal human fibroblasts, Biochem. J. 347 (2000) 543–551, https://doi.org/10.1042/0264-6021:3470543.

[45] B.G. Childs, D.J. Baker, J.L. Kirkland, J. Campisi, J.M. van Deursen, Senescence and apoptosis: dueling or complementary cell fates? EMBO Rep. 15 (2014) 1139–1153, https://doi.org/10.15252/embr.201439245.

[46] R. Banerjee, A. Mukherjee, S. Nagotu, Mitochondrial dynamics and its impact on human health and diseases: inside the DRP1 blackbox, J. Mol. Med. 100 (2022) 1–21, https://doi.org/10.1007/s00109-021-02150-7.

[47] Y.D. Du, W.Y. Guo, C.H. Han, Y. Wang, X.S. Chen, D.W. Li, J.L. Liu, M. Zhang, N. Zhu, X. Wang, N6-methyladenosine demethylase FTO impairs hepatic ischemia-reperfusion injury via inhibiting Drp1-mediated mitochondrial fragmentation, Cell Death Dis. 12 (2021) 442, https://doi.org/10.1038/s41419-021-03622-x.

[48] A. Shan, M. Li, X. Li, Y. Li, M. Yan, P. Xian, Y. Chang, X. Chen, N.J. Tang, BDE-47 decreases progesterone levels in BeWo cells by interfering with mitochondrial functions and genes related to cholesterol transport, Chem. Res. Toxicol. 32 (2019) 621–628, https://doi.org/10.1021/acs.chemrestox.8b00312.

[49] Y.J. Park, S. Lee, S. Lim, H. Nahmgoong, Y. Ji, J.Y. Huh, A.A. Alfadda, S. Kim, J. B. Kim, DNMT1 maintains metabolic fitness of adipocytes through acting as an epigenetic safeguard of mitochondrial dynamics, Proc. Natl. Acad. Sci. U. S. A. 118 (2021), https://doi.org/10.1073/pnas.2021073118.

[50] M.J. Jones, S.J. Goodman, M.S. Kobor, DNA methylation and healthy human aging, Aging Cell 14 (2015) 924–932, https://doi.org/10.1111/acel.12349.